Solar Energy Materials & Solar Cells 143 (2015) 418–423

Contents lists available at ScienceDirect

Solar Energy Materials & Solar Cells

journal homepage: www.elsevier.com/locate/solmat

Thermal cycling effect on mechanical integrity of inverted polymer solar cells

Veerle Balcaen [a], Nicholas Rolston [b], Stephanie R. Dupont [a], Eszter Voroshazi [c], Reinhold H. Dauskardt [a,*]

[a] Department of Materials Science and Engineering, Stanford University, Stanford, CA 94305-2205, USA
[b] Department of Applied Physics, Stanford University, Stanford, CA, USA
[c] IMEC vzw, Leuven, Belgium

ARTICLE INFO

Article history:
Received 16 June 2015
Received in revised form
11 July 2015
Accepted 14 July 2015
Available online 10 August 2015

Keywords:
Thermal cycling
Effective annealing
Reliability
Adhesive and cohesive failure
Meandering fracture path

ABSTRACT

The role of thermal cycling of inverted P3HT:PCBM-based polymer solar cells is reported. We found that thermal cycling between −40 °C and 85 °C up to 200 cycles had no significant effect on solar cell efficiency and mechanical integrity. On the contrary, the solar cells exhibited a slight increase in fracture resistance, similar to that reported for a post-electrode deposition thermal annealing at 85 °C. G_c increased from 2.6 J/m^2 for our control solar cells to a sustained maximum value of 4.0 J/m^2 after 25 thermal cycles. Surface analysis on the fractured samples revealed the formation of an intermixed layer between P3HT:PCBM and PEDOT:PSS, causing the debond path to change from adhesive between P3HT:PCBM and PEDOT:PSS to meandering through the intermixed layer. A kinetic analysis was used to model the effect of thermal cycling on the G_c values of polymer cells. The model revealed for cycling between −40 °C and 85 °C that 25 cycles are needed to reach the maximum G_c, which is consistent with our experimental results. After 5 thermal cycles, the effects of heating and cooling have little impact on the mechanical stability of polymer solar cells.

1. Introduction

Thermomechanical degradation of inverted polymer solar cells is of particular interest for operational reliability, particularly in light of weak internal interfaces and mechanically fragile layers [1–3]. We have recently shown how annealing temperature and time increases adhesion at the weak interface between poly(3-hexylthiophene-2,5-diyl):Phenyl-C61-butyric acid methyl ester (P3HT:PCBM) and poly(3,4-ethylenedioxythiophene) polystyrene sulfonate (PEDOT:PSS) [4]. However, the role of thermal cycling remains unclear, which is important to better understand the degradation mechanisms in operational conditions, and improve reliability and mechanical integrity in future designs. In this study we show that thermal cycling between −40 °C and 85 °C up to 200 cycles had no significant effect on solar cell efficiency and mechanical integrity, but caused a slight increase in fracture resistance, similar to that reported for a post-electrode deposition thermal annealing.

2. Experimental

2.1. Solar cell preparation

Inverted polymer solar cell devices with ITO/ZnO/P3HT:PCBM/PEDOT:PSS/Ag architecture were made on 30 mm × 30 mm square glass substrates (Fig. 1). The details of the sample preparation have been reported previously [5,6]. ZnO was spun from a zinc acetate dehydrate dissolved in 2-ethoxyethanol, ethanolamine and ethanol onto an ITO-coated glass substrate (Kintec, Kowloon, Hong Kong). A 140 nm P3HT:PCBM layer was deposited from a 1:1 wt% mixture of P3HT (Rieke Metals, Lincoln, USA) and PCBM (Solenne B.V., Groningen, Netherlands) dissolved in o-dichloro-benzene (oDCB). After deposition, all films were annealed at 130° C for 10 min in an inert atmosphere. A 30 nm PEDOT:PSS layer was deposited from a commercially available water-based dispersion (Baytron PVP AI 4083, Clevios) prior to thermal evaporation of the 100 nm Ag electrode. Finally, the solar cells were encapsulated by bonding an identical glass substrate on top of the Ag electrode using a thin brittle epoxy, resulting in a square glass sandwich.

2.2. Thermal cycling and photovoltaic characteristics

The polymer devices were subjected to thermal cycling from −40 °C to 85 °C at a heating/cooling rate of ~1.4 °C/min at the

* Corresponding author. Tel.: +1 650 725 0679; fax: +1 650 725 4034.
E-mail address: dauskardt@stanford.edu (R.H. Dauskardt).

http://dx.doi.org/10.1016/j.solmat.2015.07.019
0927-0248/

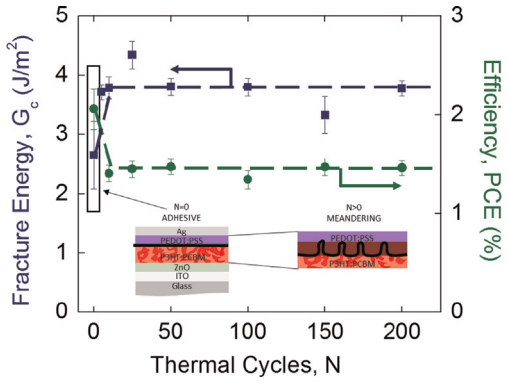

Fig. 1. The measured G_c (J/m^2) and efficiency, PCE (%) as a function of thermal cycles. Insets are illustrations of the polymer solar cell device structure with either adhesive ($N=0$) or meandering ($N>0$) failure.

highest temperature range likely to ever be encountered in service following the ISOS-T-3 protocol [7]. The minimum and maximum temperature were maintained for 15 min per cycle. The thermal cycling was performed in an environmental chamber with R.H. of 55% in the temperature range of 10–85 °C. Below 10 °C the R.H. dropped for temperatures below the dew point. Samples were removed after 5, 10, 25, 50, 100, 150 and 200 cycles. Control samples were reserved without cycling.

Photovoltaic characteristics of the thermally cycled polymer solar cells were measured in ambient atmosphere at room temperature using a two-wire configuration under a 1000 W Xenon arc lamp (Lot Oriel) with a neutral density filter (OD0.8 Newport) to obtain 100 mW cm^{-2} illumination intensity and AM1.5G spectrum. The lamp intensity was calibrated with an ISE Fraunhofer certified Si photodiode.

2.3. Adhesion specimen and testing

Double cantilever beam (DCB) adhesion specimens 5 mm wide, 30 mm long and 1.5 mm thick were diced from the encapsulated solar cells using a high-speed wafer saw with a resin blade. To prevent water coolant diffusing into the device structure and damaging the solar cell when dicing, trenches were cut on each side of the square sandwich. These trenches made it easy to cleave individual DCB specimens prior to testing. The DCB specimens were loaded under displacement control in a thin-film cohesion testing system (Delaminator DTS, Menlo Park, CA) from which a load, P, versus displacement, Δ, curve was recorded. The fracture energy, G_c (J/m^2), was measured in terms of the critical value of the applied strain energy release rate, G. G_c can be expressed in terms of the critical load, P_c, at which debond growth occurs, the debond length, a, the plain strain elastic modulus, E', of the substrates and the specimen dimensions; width, b and half-thickness, h. G_c was calculated from Eq. (1) [8]:

$$G_c = \frac{12P_c^2a^2}{B^2E'h^3}\left(1 + 0.64\frac{h}{a}\right)^2 \quad (1)$$

The debond length was measured directly under an optical microscope and also inferred from measurement of the elastic compliance, $d\Delta/dP$, using the compliance relationship in Eq. (2):

$$a = \left(\frac{d\Delta}{dP} * \frac{BE'h^3}{8}\right)^{1/3} - 0.64*h \quad (2)$$

All G_c testing was carried out in laboratory air environment at ~25 °C and ~40% R.H.

2.4. Characterization of the debond path

Following adhesion testing, a survey x-ray photo spectroscopy (XPS, PHI 5000 Versaprobe) scan (0–1000 eV) was made of each of the fractured specimens using monochromatic Al K_α x-ray radiation at 1487 eV in order to characterize the surface chemistry and to help precisely locate the debond path. The specimen half containing the Ag electrode is referred to as the "Ag side", and the other half including the ZnO is referred to as the "ZnO side". Detailed high-resolution XPS scans around the S_{2p} core level (155–175 eV) were made for compositional analysis and further identification of the debond path.

Optical and atomic force microscopy (AFM) (XE-70, Park Systems) in non-contact mode were used to characterize the surface morphology and roughness of the debond path. In addition, phase images were simultaneously collected to reveal further material properties and variations in the surface properties of the fractured cells. Ultraviolet-visible reflection measurements were performed on the Ag side of all fractured cells using an Agilent Cary 6000i UV–vis–NIR spectrophotometer to determine morphology and reorganization changes in the P3HT:PCBM layer with thermal cycling.

3. Results and discussion

3.1. Stability of thermally cycled solar cells

The power conversion efficiency (PCE) and G_c (J/m^2), measured as a function of thermal cycles, are presented in Fig. 1. G_c initially increased from ~2.6 J/m^2 for the control sample to ~4.0 J/m^2 after 25 cycles. Continued cycling up to 200 cycles had no further effect on G_c. This surprising finding is shown to be in agreement with previous reported results on post-electrode annealing [4], and will be further discussed in Section 4. Device efficiency decreased from ~2.0% to ~1.5% after the first 5 cycles and then remained constant (Fig. 1). Using Eq. (2) to measure the debond length as the crack propagated through each sample, we found that the striation regions on the fractured surfaces described in the following section occurred during loading and had slightly higher G_c values (Fig. S4). Since the laboratory testing environment was at ~40% RH, a synergistic effect of applied mechanical loads and moisture caused the crack deflection and propagation toward the PEDOT:PSS region. Previous work studied the moisture-assisted decohesion of the hydrogen bonds within PSS, where the bonds at the debond tip were strained under loading and water molecules near the tip reacted with weakened hydrogen bonds to facilitate crack growth [23]. This synergistic effect explains the different interface within the striations.

3.2. Debond path analysis

Visual inspection of both the Ag and ZnO sides of the specimens showed a clear difference in fracture path between the control and the thermally cycled samples. Control cells had uniform fractured surfaces: a gray metallic Ag side and a purple, slightly transparent ZnO side. The thermally cycled cells had fractured surfaces with striations and strong color variations over the debond length, suggesting a meandering path within the device structure (Fig. S1).

XPS survey scans of the fractured halves revealed the debond path occurred within the P3HT:PCBM and PEDOT:PSS layers for all samples. Although P3HT:PCBM and PEDOT:PSS are composed of the same elements, S_{2p} core level scans (155–175 eV) revealed their distinctive bonding structure. These scans showed a main peak